Research Article

A Functionalized Graphene Oxide–Iron Oxide Nanocomposite for Magnetically Targeted Drug Delivery, Photothermal Therapy, and Magnetic Resonance Imaging

Xinxing Ma[1,2,§], Huiquan Tao[2,§], Kai Yang[2], Liangzhu Feng[2], Liang Cheng[2], Xiaoze Shi[2], Yonggang Li[1] (✉), Liang Guo[1] (✉), and Zhuang Liu[2] (✉)

[1] Department of Radiology, the First Affiliated Hospital of Soochow University, Suzhou, Jiangsu 215006, China
[2] Jiangsu Key Laboratory for Carbon-Based Functional Materials and Devices, Institute of Functional Nano and Soft Materials Laboratory (FUNSOM), Soochow University, Suzhou, Jiangsu 215123, China

ABSTRACT

Two-dimensional graphene and its composite nanomaterials offer interesting physical/chemical properties and have been extensively explored in a wide range of fields in recent years. In this work, we synthesize a multi-functional superparamagnetic graphene oxide–iron oxide hybrid nanocomposite (GO–IONP), which is then functionalized by a biocompatible polyethylene glycol (PEG) polymer to acquire high stability in physiological solutions. A chemotherapy drug, doxorubicin (DOX), was loaded onto GO–IONP–PEG, forming a GO–IONP–PEG–DOX complex, which enables magnetically targeted drug delivery. GO–IONP–PEG also exhibits strong optical absorbance from the visible to the near-infrared (NIR) region, and can be utilized for localized photothermal ablation of cancer cells guided by the magnetic field. Moreover, for the first time, *in vivo* magnetic resonance (MR) imaging of tumor-bearing mice is also demonstrated using GO–IONP–PEG as the T_2 contrast agent. Our work suggests the promise of using multifunctional GO-based nanocomposites for applications in cancer theranostics.

KEYWORDS

1. Introduction

Graphene, a one-atom-thick two-dimensional (2D) layer of sp^2-bonded carbon, has received tremendous attention in the field of materials science because of its extraordinary electrical [1, 2], thermal [3], mechanical [4], and structural properties [5–7]. Recently, great efforts have also been devoted to explore potential applications of graphene in biomedicine [8–16]. A large number of groups have developed various graphene-based optical, electrical and electrochemical biosensors [10–13, 17–20]. We and others have utilized function-alized nanoscale graphene oxide as nanocarriers for drug and gene delivery [14, 15, 21]. Phototherapies using nano-graphene have also been demonstrated *in vitro* and *in vivo*, showing excellent tumor destruction

---

§ These authors contributed equally to this work.
Address correspondence to Zhuang Liu, zliu@suda.edu.cn; Liang Guo, ilguoliang@sohu.com; Yonggang Li, liyonggang224@163.com

effects in several animal experiments [16, 22–25]. Moreover, cytotoxicity tests of graphene and its derivatives in both cellular and animal tests [16, 26–32] have shown that although pristine graphene and as-made graphene oxide (GO) can exhibit a certain toxicity to cells and animals [26–28], functionalized nano-GO coated with biocompatible polymers such as polyethylene glycol or dextran appears to be not obviously toxic *in vitro* and *in vivo* at the tested doses [16, 29–31].

Besides pure graphene or GO, numerous graphene-based composite nanomaterials fabricated by integrating pristine graphene or GO with various types of nanoparticles have also been widely explored, showing great promise in energy research [33–35], catalysis [36, 37], electrochemical analysis [38], and other areas. Among these composite materials, GO–iron oxide nanoparticle (IONPs) composites have been synthesized by a number of groups and used for a variety of purposes [39–43]. In earlier work, Yang et al. [44] reported the use of GO–IONP as drug carriers. Recently, Chen et al. [43] demonstrated that the magnetic GO–IONP nanocomposite could also be utilized as the T_2-weighted magnetic resonance (MR) contrast agent for *in vitro* cell labeling. Despite previous efforts to explore the biomedical applications of graphene-based nanocomposite, most of the materials used in these studies were less well-functionalized (e.g., no biocompatible coating) [43, 44], and thus might not be ideal for use in biological systems. Although the use of GO–IONP for drug delivery and MR imaging has already been proposed, to the best of our knowledge, the magnetic properties of GO–IONP have not yet been fully utilized to guide drug delivery, and *in vivo* MR imaging using graphene-based nanocomposite has also not been achieved in animal experiments thus far.

In this work, a GO–IONP nanocomposite is synthesized and then functionalized by branched polyethylene glycol (PEG), giving GO–IONP–PEG with excellent stability in physiological solutions. Taking advantages of the superparamagnetic properties, high drug loading capacity, and strong optical absorption of GO–IONP–PEG, we demonstrate magnetically targeted drug delivery and photothermal therapy (PTT) *in vitro* to selectively destroy cancer cells in highly localized regions guided by the magnetic field. Furthermore, *in vivo* MR imaging of tumor-bearing mice using

GO–IONP–PEG is also realized, showing strong T_2-weighted MR contrasts in the mouse tumor and liver. The GO–IONP–PEG nanocomposite developed in this work may be a promising multifunctional nanoplatform for cancer imaging and therapy.

2. Methods and materials

2.1 Synthesis of GO–IONP

GO was made by a modified Hummers method staring from graphite. GO–IONP was fabricated following a previously reported procedure [45]. In brief, as made GO (20 mg), $FeCl_3 \cdot 6H_2O$ (270 mg), sodium acrylate (CH_2=CHCOONa, 750 mg), and sodium acetate (NaOAc, 750 mg) were dissolved in a mixture of ethylene glycol (EG, 0.5 mL) and diethylene glycol (DEG, 9.5 mL). The resulting solution was then transferred to a Teflon-lined stainless-steel autoclave, which was sealed and heated at 200 °C for 10 h. The as-prepared GO–IONP was washed several times with ethanol and deionized (D.I.) water, and dried in vacuum for 12 h. The GO:IONP weight ratio was 1:2.32 as determined by inductively coupled plasma (ICP) measurement of the Fe content.

2.2 Synthesis of GO–IONP–PEG

25 mg of 6-Arm polyethylene glycol-amine (10 kDa, SunBio Inc.) was added to a solution of GO–IONP (1 mg/mL, 5 mL) and ultrasonicated for 10 min. 5 mg of *N*-(3-dimethylaminopropyl-*N*'-ethylcarbodiimide) hydrochloride (EDC, Sigma–Aldrich) was added to the solution in two portions. The reaction solution was stirred overnight at room temperature. The resulting product (GO–IONP–PEG) was purified by centrifugation at 14,800 r/min for 10 min and washed three times with D.I. water to remove unreacted PEG and other reagents.

2.3 Determination of doxorubicin (DOX) loading and release

2.3.1 DOX loading on GO–IONP–PEG

Loading of DOX (Beijing HuaFeng United Technology Co., Ltd) onto GO–IONP–PEG was carried out by mixing different amounts of DOX (0.2 mg to

1.6 mg) with GO–IONP–PEG at a GO concentration of 0.2 mg/mL in phosphate buffer solution (PBS, 20 mmol/L) at pH 8 overnight [29, 46–48]. Unbound excess DOX was removed by centrifugation at 14,800 r/min for 10 min. The supernatant was discarded and the precipitate (GO–IONP–PEG–DOX) was washed three times with water by centrifugation. The resulting complexes were re-suspended by a brief sonication to form a homogeneous clear solution which was stored at 4 °C until use.

Ultra violet–visible–near infrared (UV–vis–NIR) spectra were recorded using a UV765 (Shanghai Precision and Scientific Instrument Co., Ltd). Fluorescence spectra of free DOX and GO–IONP–PEG–DOX were measured using a FluoroMax 4 fluorometer.

2.3.2　DOX release from GO–IONP–PEG

The GO–IONP–PEG–DOX solutions were incubated in PBS at pH 5 and 7.4 for different periods of time. DOX released from GO–IONP–PEG was collected by centrifugation at 14,800 r/min for 10 min. The amounts of released DOX in the supernatant solutions were measured by UV–vis–NIR absorbance spectroscopy.

2.4　Cellular experiments

2.4.1　Cell culture

The murine breast cancer 4T1 cell line was obtained from American Type Culture Collection (ATCC). All cell culture related reagents were purchased from HyClone. Cells were grown in normal RPMI-1640 culture medium with 10% fetal bovine serum (FBS) and 1% penicillin/streptomycin.

2.4.2　Cell cytotoxicity

The *in vitro* cytotoxicity was measured using a standard methyl thiazolyl tetrazolium (MTT, Sigma–Aldrich) assay. 4T1 cells were seeded into 96-well cell-culture plates at 5×10^4/well and then incubated for 24 h at 37 °C under 5% CO_2. After incubating 4T1 cells with various concentrations of free DOX, GO–IONP–PEG, and GO–IONP–PEG–DOX for 48 h, the standard MTT assay was carried out to determine the cell viabilities relative to the control untreated cells.

2.4.3　In vitro photothermal therapy

For photothermal cancer cell killing, 4T1 cells were incubated with 50 mg/L GO–IONP–PEG at 37 °C for 2 h. An 808 nm optical fiber-coupled diode NIR laser (maximal power = 10 W) was used to irradiate cells at a power density of 1 W/cm^2 for 5 min. A standard cell viability assay using MTT was conducted to determine the cell killing efficiency after photothermal ablation.

2.4.4　Magnetic targeting

In vitro magnetic targeting experiments were conducted by placing a magnet under the center of the cell culture dish. GO–IONP–PEG or GO–IONP–PEG–DOX added into the cell culture was concentrated to the places where the magnet was located during incubation.

2.4.5　Confocal imaging

Confocal imaging of cells was performed using a Leica SP5 laser scanning confocal microscope. The fluorescence of DOX was recorded using a 488 nm laser as the excitation source. Live and dead cells were stained by Calcein AM and propidium iodide (PI), respectively, for confocal fluorescence imaging.

2.5　MR imaging

GO–IONP–PEG solutions with concentrations ranging from 0.004 to 0.08 g/L of Fe were scanned under a 3-T clinical MRI scanner at room temperature. After acquiring the T_2-weighted MR images, the signal intensity was measured within a manually drawn region-of-interest for each sample. Relaxation rates R_2 ($R_2 = 1/T_2$) were calculated from T_2 values at different iron concentrations.

BALB/c mice (~20 g) were purchased from Nanjing Pengsheng Biological Technology Co., Ltd and used under protocols approved by Soochow University Laboratory Animal Center. For the 4T1 murine breast tumor model, ~5 × 10^6 4T1 cells in ~60 µL of serum-free RMPI-1640 medium were subcutaneously injected onto the back of each mouse. The mice were used when their tumor volumes approached 60–70 mm^3. For *in vivo* MR imaging, BALB/c mice bearing 4T1 murine breast cancer tumors were intravenously injected with GO–IONP–PEG (200 µL of 2 mg/mL solution for each mouse). MR imaging was conducted on a 3-T clinical MRI scanner equipped with a special coil designed for small animal imaging.

## 3. Results and discussion

3.1 Fabrication of GO–IONP–PEG

The GO–IONP nanocomposite was synthesized following a previously reported protocol by chemical deposition of iron oxide nanoparticles onto water-soluble GO sheets (Fig. 1(a)) [45]. X-ray diffraction (XRD) data confirmed the presence of cubic Fe_3O_4 nanocrystals on GO (see Fig. S-1 in the Electronic Supplementary Material (ESM)). As prepared GO–IONP, although soluble in water, aggregated rapidly in the presence of salts, and thus could not be directly used in biological systems (Fig. 1(b)). A branched PEG polymer, which was also used to functionalize GO in our previous studies [8, 16, 30], was covalently

conjugated to GO–IONP. The resulting GO–IONP–PEG exhibited excellent stability in various physiological solutions including saline, cell medium and serum (Fig. 1(b)). The successful PEGylation of GO–IONP–PEG was also evidenced by its infrared (IR) spectrum, in which strong C–H and C–O vibration peaks were clearly seen (see Fig. S-2 in the ESM). The optical absorbance of GO–IONP in the visible and NIR regions was significantly enhanced relative to pristine GO, likely owing to the partial reduction of GO during the formation of IONPs on GO sheets (Fig. 1(c)) [45].

The morphology of GO–IONP and GO–IONP–PEG was characterized by transmission electron microscopy (TEM). As can be seen from TEM images, IONPs with diameters of 5–10 nm were deposited on GO in the GO–IONP sample (Fig. 2(a)), and remained on the
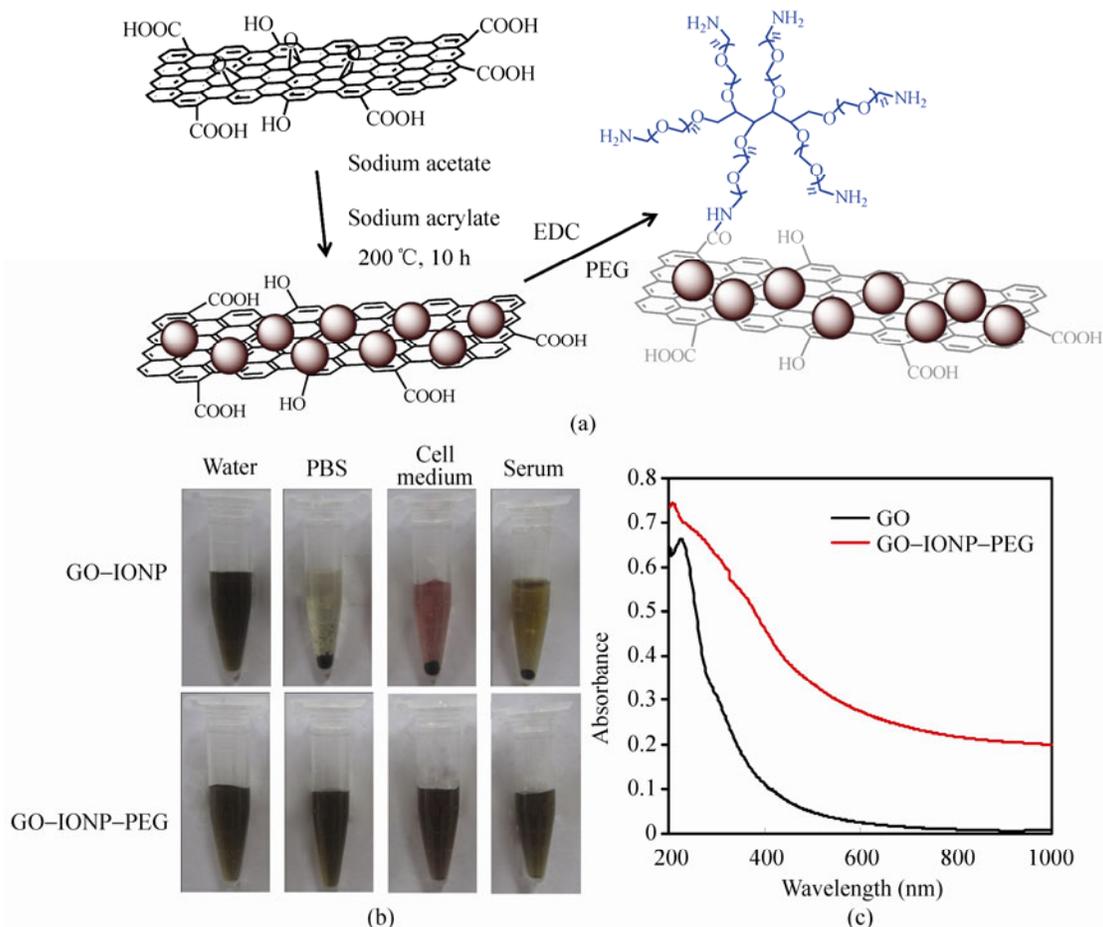
Figure 1 GO–IONP–PEG synthesis and characterization. (a) A schematic illustration of GO–IONP–PEG nanocomposite synthesis. (b) Photos of GO–IONP and GO–IONP–PEG in different solutions as indicated. GO–IONP aggregated in the presence of salts and precipitated in saline, RPMI-1640 cell medium and fetal bovine serum. (c) UV–vis–NIR absorbance spectra of GO and GO–IONP–PEG solutions at the same GO concentration (0.01 mg/mL)
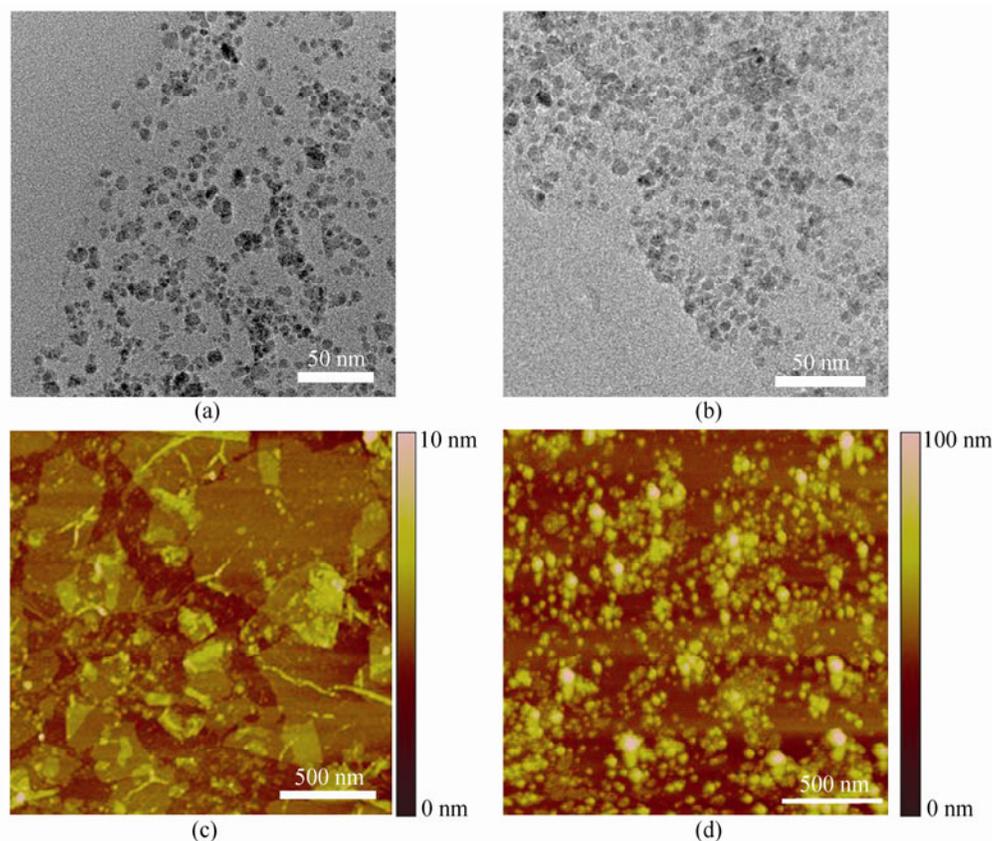
Figure 2 Microscopic characterization. TEM images of GO–IONP (a) and GO–IONP–PEG (b). The average diameter of nanoparticles grown on GO was around 10 nm. AFM images of GO (c) and GO–IONP–PEG (d). An obvious decrease in sheet size and a significant increase in sheet thickness were observed after IONP growth and PEGylation

GO sheet even after the PEGylation (Fig. 2(b)) step involving sonication of the material. Atomic force microscopy (AFM) images of GO–IONP–PEG revealed that their sheet sizes were much smaller than that of as-made GO, and showed a relatively large distribution ranging from ~50 nm to ~300 nm (Figs. 2(c) and 2(d)).

3.2   Magnetic properties of GO–IONP–PEG

Photos of GO–IONP–PEG in aqueous solutions with and without a magnet clearly demonstrated its excellent magnetic properties (Fig. 3(a)). The magnetization hysteresis loop further indicated the superparamagnetic nature of GO–IONP–PEG (Fig. 3(b)). IONPs have been widely used as the T_2-contrast agent in MR imaging [49–51]. T_2-weighted MR images (Fig. 3(c)) of GO–IONP–PEG solutions acquired on a 3-T MR scanner revealed the concentration-dependent darkening effect. The transverse relaxivity (r_2) of GO–IONP–PEG was measured to be 60 L·mmol^{-1}·S^{-1} (Fig. 3(d)).
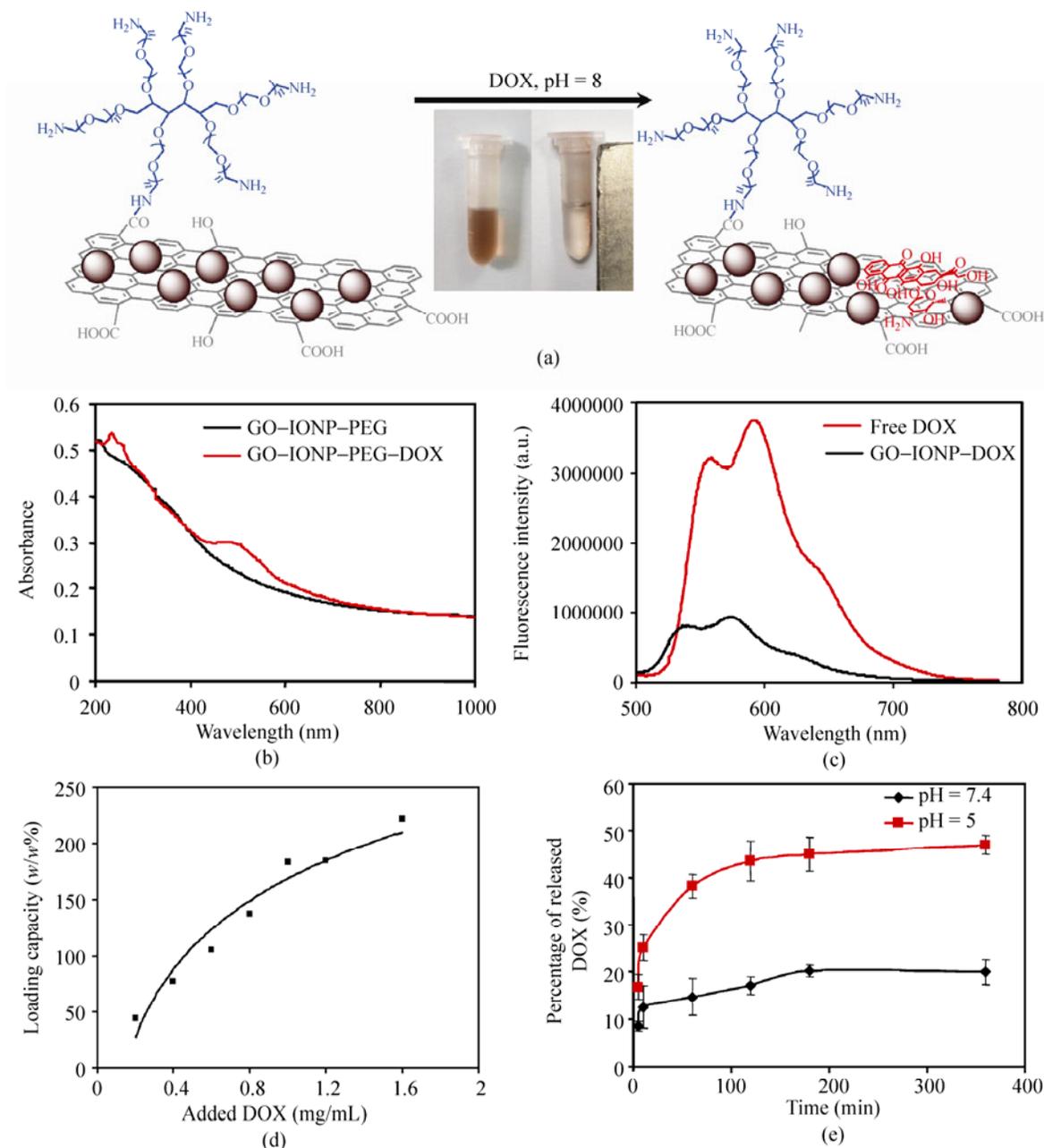
3.3   Drug loading and release with GO–IONP–PEG

Our and others' previous studies have shown that aromatic molecules including many chemotherapy drugs may be loaded on the surface of sp^2-carbon nano-materials such as carbon nanotubes and graphene by π–π stacking [29, 47, 48, 52]. In this work, DOX, a commonly used anti-cancer drug, was loaded on GO–IONP–PEG via the same method (Fig. 4(a)). The DOX loaded GO–IONP–PEG (GO–IONP–PEG–DOX) was readily dispersed in water, forming a clear transparent solution with reddish color (Fig. 4(a), inset). The loading of DOX in the GO–IONP–PEG–DOX sample was also evidenced from the characteristic UV–vis absorbance peak of DOX at 490 nm superimposed on the GO–IONP–PEG absorption spectrum (Fig. 4(b)). As expected, a significant DOX fluorescence quenching effect in the GO–IONP–PEG–DOX sample was observed (Fig. 4(c)), likely due to the close binding between DOX molecules and the graphene surface [46, 52].
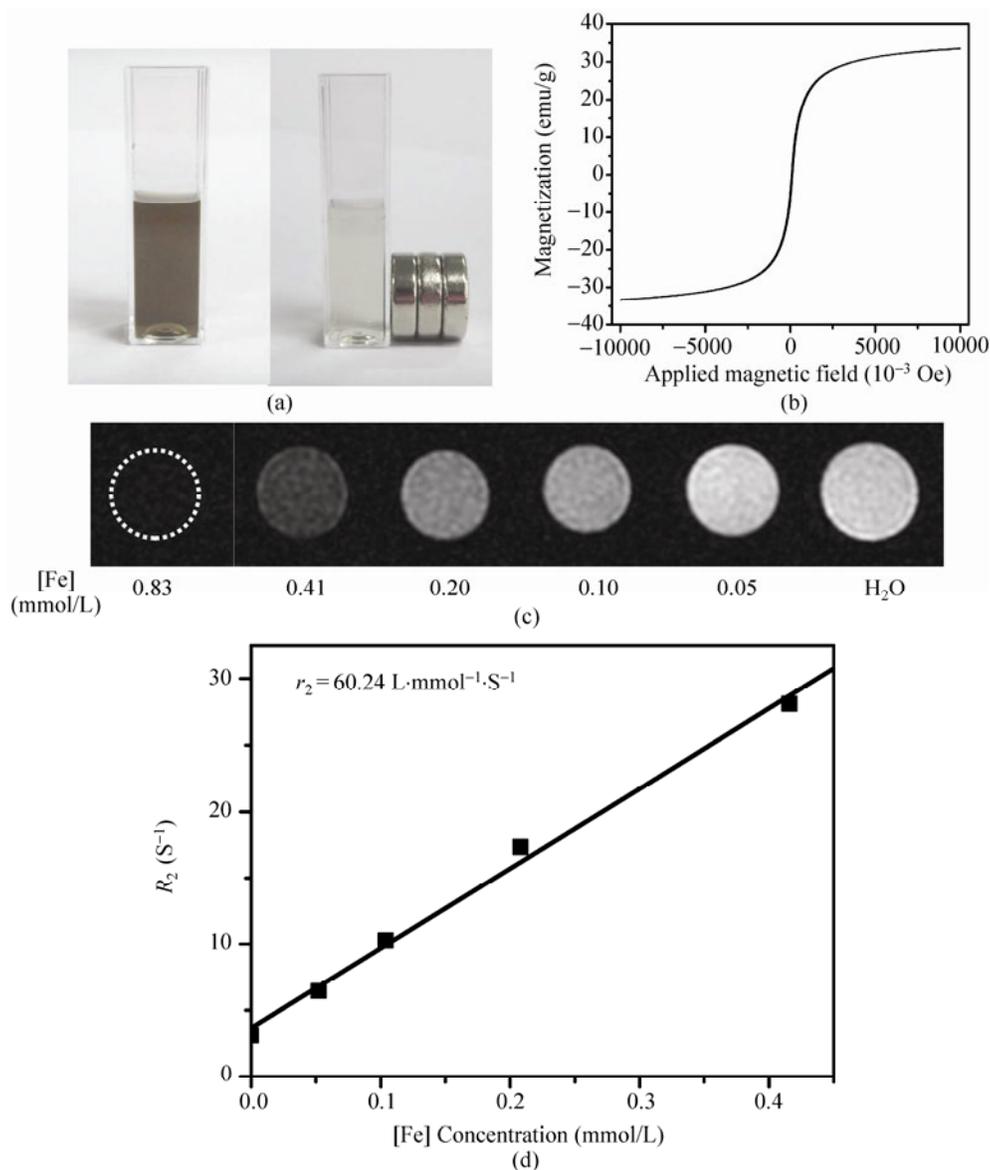
Figure 3   Magnetic properties of GO–IONP–PEG. (a) Photos of GO–IONP–PEG in aqueous solutions with and without a magnet. (b) Magnetization loops of GO–IONP–PEG. The absence of a hysteresis loop indicates the superparamagnetic properties of GO–IONP–PEG. (c) T_2-weighted MR images of GO–IONP–PEG solutions at different iron concentrations. (d) T_2 relaxation rates (R_2) of GO–IONP–PEG solutions at different iron concentrations

To determine the saturation level of DOX loading onto GO–IONP–PEG, GO–IONP–PEG solutions were added with different amounts of DOX at pH 8.0. After removal of excess unbound DOX, it was found that the DOX loading efficiency increased from 44% to ~220% (the weight ratio of DOX to GO) with increasing amount of added DOX (Fig. 4(d)). A DOX loading of ~100% (using a GO:DOX weight ratio of 1:2) for GO–IONP–PEG–DOX was chosen for the followed experiments.

To understand the drug release behaviors of GO–IONP–PEG–DOX at neutral and acidic pH, we incubated GO–IONP–PEG–DOX in pH 7.4 and 5.0 phosphate buffers [53] (Fig. 4(e)). The released DOX from GO–IONP–PEG was measured by fluorescence spectroscopy of supernatants from GO–IONP–PEG–DOX after centrifugation at different time points. Within 360 min, about 20% of DOX was released from the nanocomposite at pH 7.4, while nearly 50% of DOX was released in the acidic buffer at pH 5.0, owing to the

Figure 4 Drug loading and release in the GO–IONP–PEG–DOX system. (a) A schematic illustration of GO–IONP–PEG loaded with DOX. Inset: photos of GO–IONP–PEG–DOX in aqueous solutions with and without a magnet. (b) UV–vis–NIR absorbance spectra of GO–IONP–PEG and GO–IONP–PEG–DOX. (c) Fluorescence spectra of free DOX and GO–IONP–DOX at the same DOX concentration (5 μmol/L) under 490 nm excitation. (d) Quantification of DOX loading at different feeding amounts of DOX. The GO concentration was kept at 0.2 mg/mL in GO–IONP–PEG samples. A maximal DOX loading of ~220% by weight was obtained in the experiment. (e) DOX release from GO–IONP–PEG–DOX nanocomposite in buffers at pH 5.0 and 7.4 at different time points. Error bars are based on triplicate samples

protonation of the amino group in the DOX molecule that gives DOX a positive charge, weakening its interaction with the hydrophobic graphene surface, and thus triggering drug release. However, an appreciable burst release (~10% at pH 7.4 in the first few minutes) was noticed in our GO–IONP–PEG–DOX system. This issue may potentially be resolved by further designing and engineering the surface chemistry of our nanocarrier system (e.g., polymer cross-linking on the GO–IONP surface).

3.4 *In vitro* toxicity

Standard MTT cell viability assay was performed to compare the cytotoxicity of GO–IONP–PEG–DOX and free DOX at series of DOX concentrations to 4T1 cells (Fig. 5(a)). The half-maximum inhibitory concentration (IC50) value for GO–IONP–PEG–DOX was found to be 0.52 μmol/L, which was comparable to that of free DOX at 0.43 μmol/L. Importantly, GO–IONP–PEG without drug loading exhibited no appreciable toxicity to treated cells even at high concentrations up to 0.16 mg/mL (Fig. 5(b)).

3.5 Magnetically targeted drug delivery

Drug delivery under magnetic targeting has been reported by a number of groups in recent years [54–56]. Many studies have shown that magnetic nanoparticles can be retained at tumor sites by a locally applied external magnetic field, thereby enabling magnetic tumor targeting [56–58]. The excellent magnetic properties of GO–IONP–PEG allow us to use it as a nanocarrier for magnetically targeted drug delivery.

In our experiments, a magnet was placed under the cell culture dish, inducing an apparent local accumulation of added GO–IONP–PEG–DOX guided by the magnetic field (Fig. 6(a)). Confocal fluorescence images detecting DOX fluorescence revealed the high uptake of GO–IONP–PEG–DOX by cells grown right above the magnet, with little DOX fluorescence in cells far from the magnet in the same culture dish,

after 6 h of incubation. Calcein AM/PI double stained images of cells after 24 h of incubation further showed that the magnetically targeted drug delivery by GO–IONP–PEG–DOX was able to selectively kill cells that were localized close to the magnet, without affecting the viability of cells outside the magnetic field (Fig. 6(c)). In contrast, GO–IONP–PEG was not toxic to cells under the magnetic field (Fig. S-3 in the ESM).

3.6 Magnetically targeted photothermal therapy

PTT usually employs light-absorbing agents to induce photothermal damage of tumor cells under exposure to NIR light [59]. In recent years, many nanomaterials including various nanostructures, carbon nanotubes, and nano-graphene have been under investigation for PTT treatment of cancer [16, 59–61]. Owing to its strong optical absorption in the NIR window, GO–IONP–PEG was also utilized for photothermal ablation of cancer cells in this work. When exposed to an 808 nm NIR laser at a power density of 1 W/cm^2, the temperature of GO–IONP–PEG rapidly increased following a concentration-dependent manner, in marked contrast to the negligible temperature change of water under the same irradiation conditions (Fig. 7(a)).

The photothermal effect of GO–IONP–PEG was then used for photothermal ablation of cancer cells. 4T1 cells were incubated with GO–IONP–PEG for 2 h, and then exposed to an 808 nm laser at different power
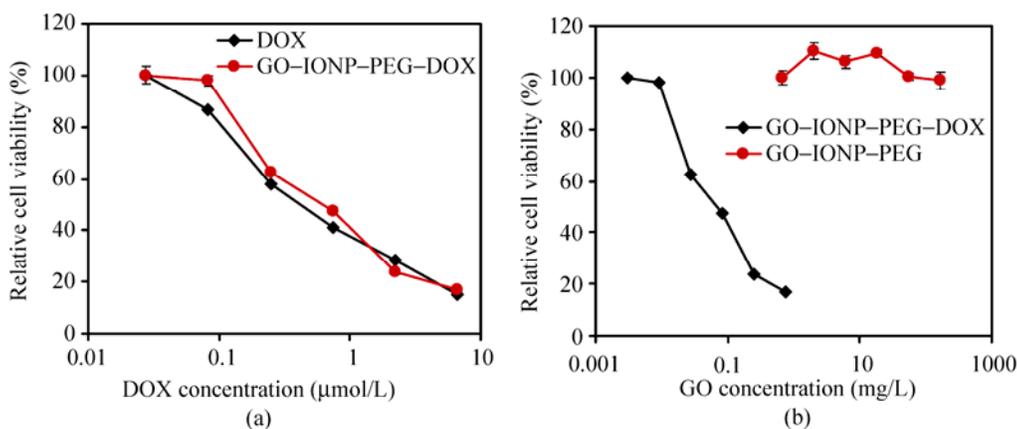
Figure 5 *In vitro* cell toxicity experiments. (a) Relative viabilities of 4T1 cells after being incubated with various concentrations of free DOX and GO–IONP–PEG–DOX for 24 h. (b) Relative viabilities of 4T1 cells after being incubated with various concentrations of GO–IONP–PEG and GO–IONP–PEG–DOX for 24 h. While GO–IONP–PEG was not obviously toxic to cells even at very high concentrations, GO–IONP–PEG–DOX exhibited similar cytotoxicity to free DOX. Error bars are based on triplicate samples
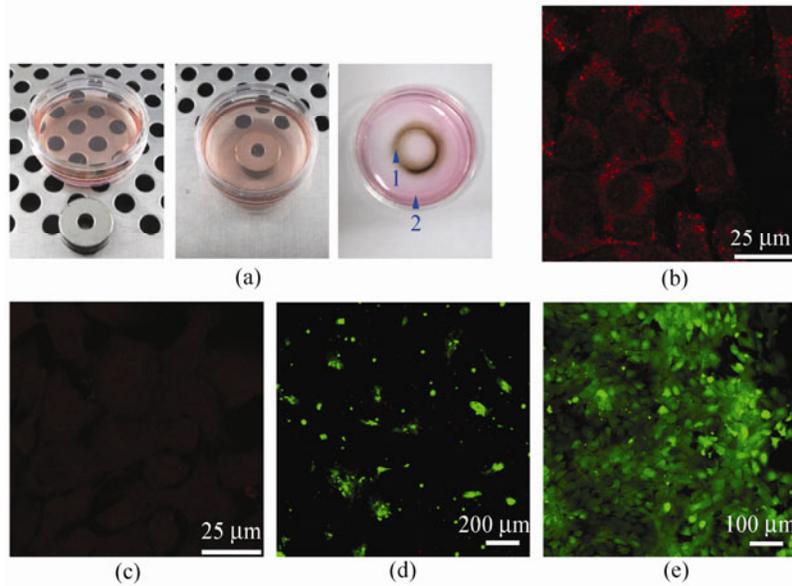
Figure 6 Magnetically targeted drug delivery. (a) Photos of 4T1 cells incubated with GO–IONP–PEG–DOX with and without a magnet. Confocal images of GO–IONP–PEG–DOX incubated cells incubated taken right above the magnet (b) and far from the magnet (c). DOX fluorescence was detected in these images, which were acquired after 6 h of incubation. Confocal images of Calcein AM/PI co-stained cells after being incubated with GO–IONP–PEG–DOX for 24 h with images taken right above the magnet (d) and far from the magnet (e). Live and dead cells were stained green and red colors under the fluorescence microscope, by Calcein AM and PI, respectively
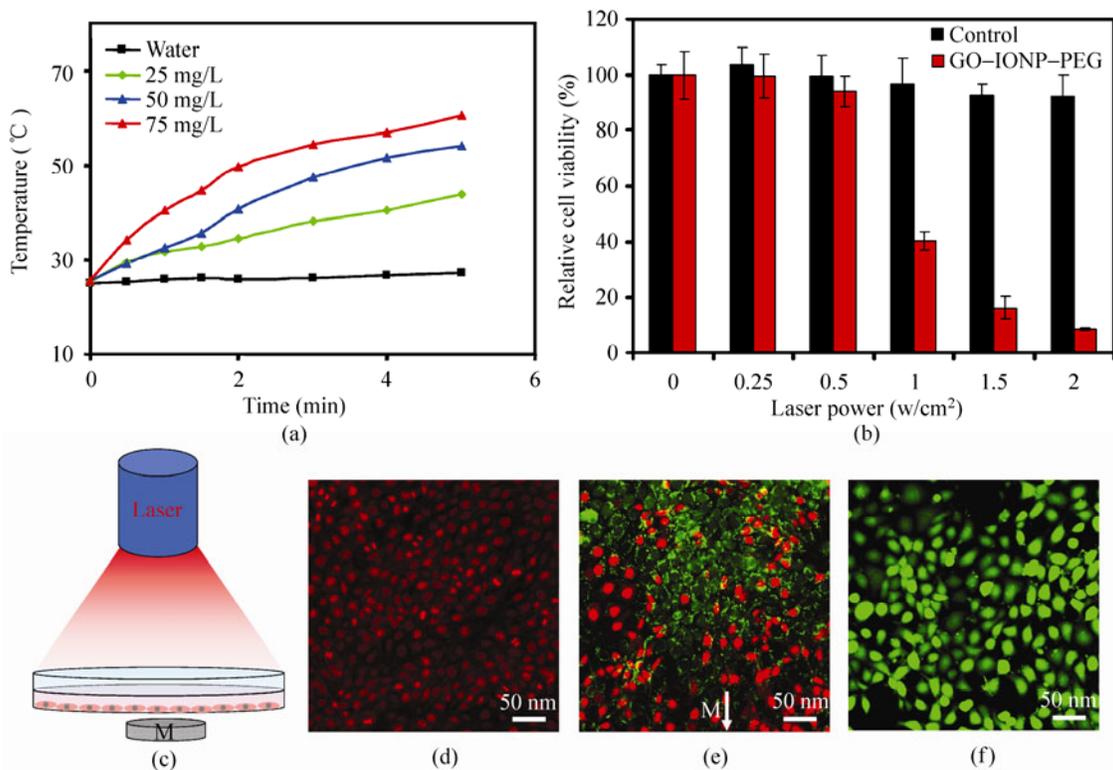

Figure7 Magnetically targeted photothermal ablation of cancer cells. (a) Temperature changes of water and different concentrations of GO–IONP–PEG (25, 50, 75 mg/L) under 808 nm laser irradiation at a power density of 1 W/cm^2 for 5 min; (b) Relative viabilities of GO–IONP–PEG (50 mg/L) treated 4T1 cells and untreated control cells after being irradiated with the NIR laser at different power densities for 5 min. (c) A scheme showing magnetically targeted photothermal therapy. A magnet was placed under the cell culture dish during incubation. Confocal fluorescence images of calcein AM (green, live cells) and PI (red, dead cells) co-stained cells after magnetically targeted photothermal ablation with the images taken at three different locations in the culture dish: (d) right above the magnet; (e) close to the magnet; (f) far from the magnet. Error bars are based on four parallel samples

densities for 5 min. MTT assay was carried out to determine relative viabilities of cells post-PTT treatment. It was found that while the viabilities of untreated cells were not noticeably affected even under high power laser irradiation (up to 2 W/cm²), GO–IONP–PEG incubated cancer cells were largely killed after laser irradiation, showing decreasing cell viabilities as the laser power was increased (Fig. 7(b)). The magnetic properties of GO–IONP–PEG can be further utilized for magnetically targeted PTT. 4T1 cells were incubated with GO–IONP–PEG for 2 h at 37 °C in the presence of a magnetic field. After being exposed to the NIR laser for 20 min, cells near the magnet were effectively destroyed, while those far from the magnet were essentially unaffected (Fig. 7(c)).

3.7 *In vivo* MR imaging

Although several groups have proposed the use of GO–IONP nanocomposites for MR imaging, no real animal imaging results have been presented so far to our best knowledge, likely due to the lack of biocompatible surface coatings in many of previously reported GO–IONP nanocomposites [41, 43]. In our study, we conducted whole-body animal imaging by intravenously injecting GO–IONP–PEG into 4T1 tumor-bearing BALB/c mice, which were imaged under a 3-T clinical MR scanner one day after injection. T_2-weighted MR images of GO–IONP–PEG injected mice showed dramatic darkening effects in the tumor and liver areas (Figs. 8(a) and 8(b)), with signals significantly decreased by ~67% and ~64% (Figs. 8(c) and 8(d)),
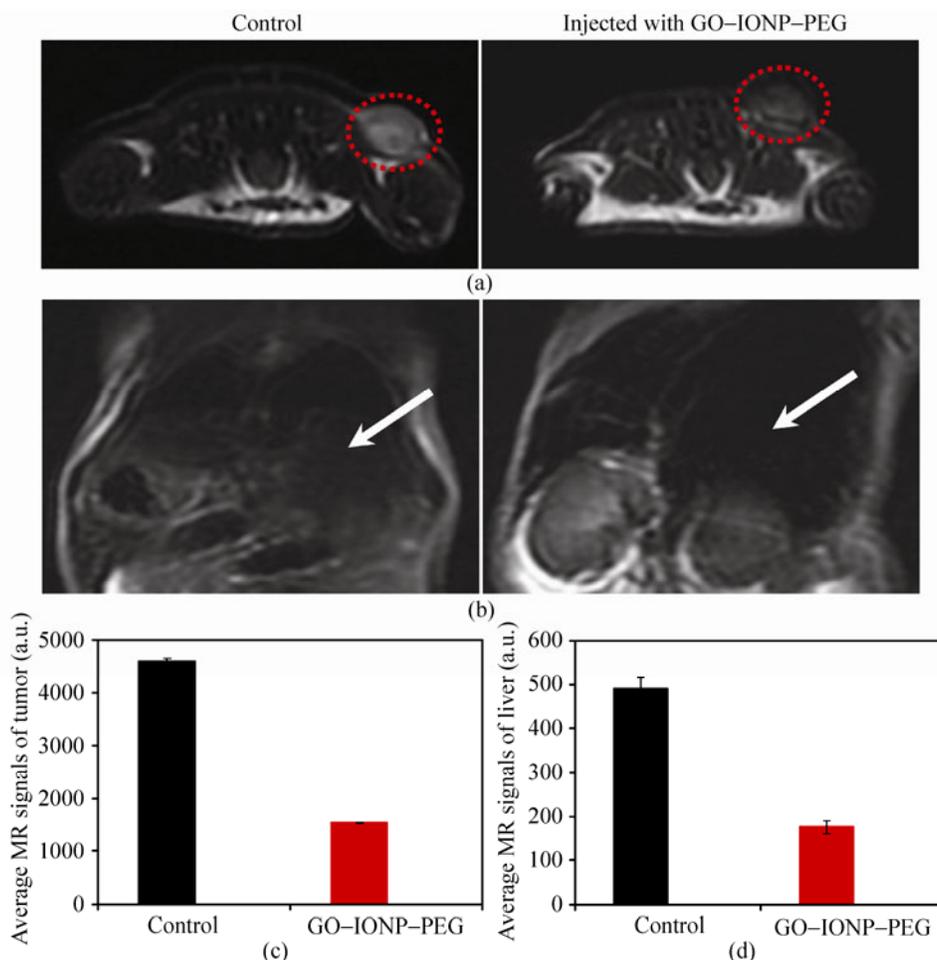
Figure 8 *In vivo* MR imaging. Transversal (a) and longitudinal (b) T_2-weighted MR images of 4T1 tumor-bearing mice with (right) and without (left) GO–IONP–PEG injection. Images were taken 24 h after intravenous injection. Tumor and liver in these images are highlighted by red circles and white arrows, respectively. Quantification of T_2-weighted MR signals from the tumor (c) and liver (d) of mice with and without GO–IONP–PEG injection. Error bars are based on three animals per group

respectively, as compared with untreated control mice. Our MR imaging data suggest high tumor uptake of GO–IONP–PEG, similar to the behavior of PEGylated GO reported in our previous study and is likely due to the enhanced permeability and retention effect of cancerous tumors [16, 25]. The liver accumulation of GO–IONP–PEG is expected as a result of macrophage uptake of nanomaterials in reticuloendothelial systems (RES). Although further careful studies are required to understand the detailed *in vivo* pharmacokinetics, biodistribution and toxicology of our GO–IONP–PEG, this is the first demonstration of the use of graphene-based composite nanomaterials for *in vivo* MR imaging of animals.

4. Conclusions

We have developed a multi-functional magnetic nanoparticle-decorated GO nanocomposite with biocompatible surface functionalization. The GO–IONP–PEG was stable in physiological environments and exhibited no obvious *in vitro* toxicity to cells at the tested concentrations. Drug delivery and photothermal treatment targeted under a magnetic field was further realized using GO–IONP–PEG, achieving selective killing of cancer cells in highly localized regions. Last but not least, *in vivo* MR imaging of tumors in mice was also demonstrated using our GO–IONP–PEG as the T_2 contrast agent. In future studies, the magnetically targeted drug delivery and photothermal treatment will be combined together in an attempt to further enhance therapeutic efficacy. Studies on MR imaging and guided novel cancer therapies using GO–IONP–PEG are also ongoing in our laboratory. This work presents a simple approach to prepare a graphene-based biocompatible nanocomposite with multiple functionalities and great potential in cancer theranostics.

References

[1] Novoselov, K. S.; Jiang, Z.; Zhang, Y.; Morozov, S. V.; Stormer, H. L.; Zeitler, U.; Maan, J. C.; Boebinger, G. S.; Kim, P.; Geim, A. K. Room-temperature quantum Hall effect in graphene. *Science* **2007**, *315*, 1379.

[2] Zhang, Y. B.; Tan, Y. W.; Stormer, H. L.; Kim, P. Experimental observation of the quantum Hall effect and Berry's phase in graphene. *Nature* **2005**, *438*, 201–204.

[3] Balandin, A. A.; Ghosh, S.; Bao, W.; Calizo, I.; Teweldebrhan, D.; Miao, F.; Lau, C. N. Superior thermal conductivity of single-layer graphene. *Nano Lett.* **2008**, *8*, 902–907.

[4] Lee, C.; Wei, X.; Kysar, J. W.; Hone, J. Measurement of the elastic properties and intrinsic strength of monolayer graphene. *Science* **2008**, *321*, 385–388.

[5] Meyer, J. C.; Geim, A. K.; Katsnelson, M. I.; Novoselov, K. S.; Booth, T. J.; Roth, S. The structure of suspended graphene sheets. *Nature* **2007**, *446*, 60–63.

[6] Huang, X.; Yin, Z.; Wu, S.; Qi, X.; He, Q.; Zhang, Q.; Yan, Q.; Boey, F.; Zhang, H. Graphene-based materials: Synthesis, characterization, properties, and applications. *Small* **2011**, *7*, 1876–1902.

[7] Huang, X.; Qi, X.; Boey, F.; Zhang, H. Graphene-based composites. *Chem. Soc. Rev.* **2012**, *41*, 666–686.

[8] Liu, Z.; Robinson, J. T.; Sun, X.; Dai, H. PEGylated nanographene oxide for delivery of water-insoluble cancer drugs. *J. Am. Chem. Soc.* **2008**, *130*, 10876–10877.

[9] Feng, L. Z.; Liu, Z. A. Graphene in biomedicine: Opportunities and challenges. *Nanomedicine* **2011**, *6*, 317–324.

[10] He, Q. Y.; Sudibya, H. G.; Yin, Z. Y.; Wu, S. X.; Li, H.; Boey, F.; Huang, W.; Chen, P.; Zhang, H. Centimeter-long and large-scale micropatterns of reduced graphene oxide films: Fabrication and sensing applications. *ACS Nano* **2010**, *4*, 3201–3208.

[11] Sudibya, H. G.; He, Q. Y.; Zhang, H.; Chen, P. Electrical detection of metal ions using field-effect transistors based

on micropatterned reduced graphene oxide films. *ACS Nano* **2011**, *5*, 1990–1994.

[12] He, S.; Song, B.; Li, D.; Zhu, C.; Qi, W.; Wen, Y.; Wang, L.; Song, S.; Fang, H.; Fan, C. A graphene nanoprobe for rapid, sensitive, and multicolor fluorescent DNA analysis. *Adv. Funct. Mater.* **2010**, *20*, 453–459.

[13] Tang, L. A. L.; Wang, J.; Loh, K. P. Graphene-based SELDI probe with ultrahigh extraction and sensitivity for DNA oligomer. *J. Am. Chem. Soc.* **2010**, *132*, 10976–10977.

[14] Feng, L.; Zhang, S.; Liu, Z. Graphene based gene transfection. *Nanoscale* **2011**, *3*, 1252–1257.

[15] Zhang, L.; Xia, J.; Zhao, Q.; Liu, L.; Zhang, Z. Functional graphene oxide as a nanocarrier for controlled loading and targeted delivery of mixed anticancer drugs. *Small* **2010**, *6*, 537–544.

[16] Yang, K.; Zhang, S.; Zhang, G.; Sun, X.; Lee, S. T.; Liu, Z. Graphene in mice: Ultrahigh *in vivo* tumor uptake and efficient photothermal therapy. *Nano Lett.* **2010**, *10*, 3318–3323.

[17] Yin, Z.; He, Q.; Huang, X.; Zhang, J.; Wu, S.; Chen, P.; Lu, G.; Chen, P.; Zhang, Q.; Yan, Q.; Zhang, H. Real-time DNA detection using Pt nanoparticle-decorated reduced graphene oxide field-effect transistors. *Nanoscale* **2012**, *4*, 293–297.

[18] Wang, Z.; Zhang, J.; Chen, P.; Zhou, X.; Yang, Y.; Wu, S.; Niu, L.; Han, Y.; Wang, L.; Chen, P.; Boey, F.; Zhang, Q.; Liedberg, B.; Zhang, H. Label-free, electrochemical detection of methicillin-resistant *Staphylococcus aureus* DNA with reduced graphene oxide-modified electrodes. *Biosens. Bioelectron.* **2011**, *26*, 3881–3886.

[19] Wang, Z.; Zhou, X.; Zhang, J.; Boey, F.; Zhang, H. Direct electrochemical reduction of single-layer graphene oxide and subsequent functionalization with glucose oxidase. *J. Phys. Chem. C* **2009**, *113*, 14071–14075.

[20] Peng, C.; Jiang, B.; Liu, Q.; Guo, Z.; Xu, Z.; Huang, Q.; Xu, H.; Tai, R.; Fan, C. Graphene-templated formation of two-dimensional lepidocrocite nanostructures for high-efficiency catalytic degradation of phenols. *Energy Environ. Sci.* **2011**, *4*, 2035–2040.

[21] Tian, B.; Wang, C.; Zhang, S.; Feng, L. Z.; Liu, Z. Photothermally enhanced photodynamic therapy delivered by nano-graphene oxide. *ACS Nano* **2011**, *5*, 7000–7009.

[22] Robinson, J. T.; Tabakman, S. M.; Liang, Y. Y.; Wang, H. L.; Casalongue, H. S.; Vinh, D.; Dai, H. J. Ultrasmall reduced graphene oxide with high near-infrared absorbance for photothermal therapy. *J. Am. Chem. Soc.* **2011**, *133*, 6825–6831.

[23] Zhang, W.; Guo, Z. Y.; Huang, D. Q.; Liu, Z. M.; Guo, X.; Zhong, H. Q. Synergistic effect of chemo-photothermal therapy using PEGylated graphene oxide. *Biomaterials* **2011**, *32*, 8555–8561.

[24] Markovic, Z. M.; Harhaji-Trajkovic, L. M.; Todorovic-Markovic, B. M.; Kepic, D. P.; Arsikin, K. M.; Jovanovic, S. P.; Pantovic, A. C.; Dramicanin, M. D.; Trajkovic, V. S. *In vitro* comparison of the photothermal anticancer activity of graphene nanoparticles and carbon nanotubes. *Biomaterials* **2011**, *32*, 1121–1129.

[25] Yang, K.; Wan, J.; Zhang, S.; Tian, B.; Zhang, Y.; Liu, Z. The influence of surface chemistry and size of nanoscale graphene oxide on photothermal therapy of cancer using ultra-low laser power. *Biomaterials,* in press, **2012**, DOI: 10.1016/j.biomaterials.2011.11.064.

[26] Zhang, Y. B.; Ali, S. F.; Dervishi, E.; Xu, Y.; Li, Z. R.; Casciano, D.; Biris, A. S. Cytotoxicity effects of graphene and single-wall carbon nanotubes in neural phaeochromocytoma-derived PC12 cells. *ACS Nano* **2010**, *4*, 3181–3186.

[27] Wang, K.; Ruan, J.; Song, H.; Zhang, J.; Wo, Y.; Guo, S.; Cui, D. Biocompatibility of graphene oxide. *Nanoscale Res. Lett.* **2011**, *6*, 8.

[28] Duch, M. C.; Budinger, G. R. S.; Liang, Y. T.; Soberanes, S.; Urich, D.; Chiarella, S. E.; Campochiaro, L. A.; Gonzalez, A.; Chandel, N. S.; Hersam, M. C.; Mutlu, G. M. Minimizing oxidation and stable nanoscale dispersion improves the biocompatibility of graphene in the lung. *Nano Lett.* **2011**, *11*, 5201–5207.

[29] Sun, X.; Liu, Z.; Welsher, K.; Robinson, J. T.; Goodwin, A.; Zaric, S.; Dai, H. Nano-graphene oxide for cellular imaging and drug delivery. *Nano Res.* **2008**, *1*, 203–212.

[30] Yang, K.; Wan, J. M.; Zhang, S. A.; Zhang, Y. J.; Lee, S. T.; Liu, Z. A. *In vivo* pharmacokinetics, long-term biodistribution, and toxicology of PEGylated graphene in mice. *ACS Nano* **2011**, *5*, 516–522.

[31] Zhang, S. A.; Yang, K.; Feng, L. Z.; Liu, Z. *In vitro* and *in vivo* behaviors of dextran functionalized graphene. *Carbon* **2011**, *49*, 4040–4049.

[32] Agarwal, S.; Zhou, X.; Ye, F.; He, Q.; Chen, G. C. K.; Soo, J.; Boey, F.; Zhang, H.; Chen, P. Interfacing live cells with nanocarbon substrates. *Langmuir* **2010**, *26*, 2244–2247.

[33] Wang, H. L.; Liang, Y. Y.; Mirfakhrai, T.; Chen, Z.; Casalongue, H. S.; Dai, H. J. Advanced asymmetrical supercapacitors based on graphene hybrid materials. *Nano Res.* **2011**, *4*, 729–736.

[34] Wang, P.; Jiang, T. F.; Zhu, C. Z.; Zhai, Y. M.; Wang, D. J.;

Dong, S. J. One-step, solvothermal synthesis of graphene–CdS and graphene–ZnS quantum dot nanocomposites and their interesting photovoltaic properties. *Nano Res.* **2010**, *3*, 794–799.

[35] Cao, X.; Shi, Y.; Shi, W.; Lu, G.; Huang, X.; Yan, Q.; Zhang, Q.; Zhang, H. Preparation of novel 3D graphene networks for supercapacitor applications. *Small* **2011**, *7*, 3163–3168.

[36] Xu, C.; Wang, X.; Zhu, J. Graphene–metal particle nano-composites. *J. Phys. Chem. C* **2008**, *112*, 19841–19845.

[37] Liang, Y. Y.; Wang, H. L.; Casalongue, H. S.; Chen, Z.; Dai, H. J. TiO$_2$ nanocrystals grown on graphene as advanced photocatalytic hybrid materials. *Nano Res.* **2010**, *3*, 701–705.

[38] Shan, C.; Yang, H.; Song, J.; Han, D.; Ivaska, A.; Niu, L. Direct electrochemistry of glucose oxidase and biosensing for glucose based on graphene. *Anal. Chem.* **2009**, *81*, 2378–2382.

[39] Liang, J.; Xu, Y.; Sui, D.; Zhang, L.; Huang, Y.; Ma, Y.; Li, F.; Chen, Y. Flexible, magnetic, and electrically conductive graphene/Fe$_3$O$_4$ paper and its application for magnetic-controlled switches. *J. Phys. Chem. C* **2010**, *114*, 17465–17471.

[40] Zhou, G.; Wang, D. W.; Li, F.; Zhang, L.; Li, N.; Wu, Z. S.; Wen, L.; Lu, G. Q.; Cheng, H. M. Graphene-wrapped Fe$_3$O$_4$ anode material with improved reversible capacity and cyclic stability for lithium ion batteries. *Chem. Mater.* **2010**, *22*, 5306–5313.

[41] Cong, H. P.; He, J. J.; Lu, Y.; Yu, S. H. Water-soluble magnetic-functionalized reduced graphene oxide sheets: *In situ* synthesis and magnetic resonance imaging applications. *Small* **2010**, *6*, 169–173.

[42] Ji, L.; Tan, Z.; Kuykendall, T. R.; Aloni, S.; Xun, S.; Lin, E.; Battaglia, V.; Zhang, Y. Fe$_3$O$_4$ nanoparticle-integrated graphene sheets for high-performance half and full lithium ion cells. *Phys. Chem. Chem. Phys.* **2011**, *13*, 7170–7177.

[43] Chen, W.; Yi, P.; Zhang, Y.; Zhang, L.; Deng, Z.; Zhang, Z. Composites of aminodextran-coated Fe$_3$O$_4$ nanoparticles and graphene oxide for cellular magnetic resonance imaging. *ACS Appl. Mater. Interf.* **2011**, *3*, 4085–4091.

[44] Yang, X.; Zhang, X.; Ma, Y.; Huang, Y.; Wang, Y.; Chen, Y. Superparamagnetic graphene oxide-Fe$_3$O$_4$ nanoparticles hybrid for controlled targeted drug carriers. *J. Mater. Chem.* **2009**, *19*, 2710–2714.

[45] Sun, H.; Cao, L.; Lu, L. Magnetite/reduced graphene oxide nanocomposites: One step solvothermal synthesis and use as a novel platform for removal of dye pollutants. *Nano Res.*

2011, *4*, 550–562.

[46] Wang, C.; Cheng, L.; Liu, Z. Drug delivery with upconversion nanoparticles for multi-functional targeted cancer cell imaging and therapy. *Biomaterials* **2011**, *32*, 1110–1120.

[47] Liu, Z.; Fan, A. C.; Rakhra, K.; Sherlock, S.; Goodwin, A.; Chen, X.; Yang, Q.; Felsher, D. W.; Dai, H. Supramolecular stacking of doxorubicin on carbon nanotubes for *in vivo* cancer therapy. *Angew. Chem Int. Ed.* **2009**, *48*, 7668–7672.

[48] Sherlock, S. P.; Dai, H. Multifunctional FeCo–graphitic carbon nanocrystals for combined imaging, drug delivery and tumor-specific photothermal therapy in mice. *Nano Res.* **2011**, *4*, 1248–1260.

[49] Na, H. B.; Song, I. C.; Hyeon, T. Inorganic nanoparticles for MRI contrast agents. *Adv. Mater.* **2009**, *21*, 2133–2148.

[50] Wang, L.; Neoh, K. G.; Kang, E. T.; Shuter, B.; Wang, S. C. Superparamagnetic hyperbranched polyglycerol-grafted Fe$_3$O$_4$ nanoparticles as a novel magnetic resonance imaging contrast agent: An *in vitro* assessment. *Adv. Funct. Mater.* **2009**, *19*, 2615–2622.

[51] Ai, H.; Flask, C.; Weinberg, B.; Shuai, X. T.; Pagel, M. D.; Farrell, D.; Duerk, J.; Gao, J. Magnetite-loaded polymeric micelles as ultrasensitive magnetic-resonance probes. *Adv. Mater.* **2005**, *17*, 1949–1952.

[52] Liu, Z.; Sun, X. M.; Nakayama-Ratchford, N.; Dai, H. J. Supramolecular chemistry on water-soluble carbon nanotubes for drug loading and delivery. *ACS Nano* **2007**, *1*, 50–56.

[53] Xu, H.; Cheng, L.; Wang, C.; Ma, X.; Li, Y.; Liu, Z. Polymer encapsulated upconversion nanoparticle/iron oxide nanocomposites for multimodal imaging and magnetic targeted drug delivery. *Biomaterials* **2011**, *32*, 9364–9373.

[54] Veiseh, O.; Gunn, J. W.; Zhang, M. Design and fabrication of magnetic nanoparticles for targeted drug delivery and imaging. *Adv. Drug Deliv. Rev.* **2010**, *62*, 284–304.

[55] Chertok, B.; Moffat, B. A.; David, A. E.; Yu, F.; Bergemann, C.; Ross, B. D.; Yang, V. C. Iron oxide nanoparticles as a drug delivery vehicle for MRI monitored magnetic targeting of brain tumors. *Biomaterials* **2008**, *29*, 487–496.

[56] Cheng, L.; Yang, K.; Li, Y.; Chen, J.; Wang, C.; Shao, M.; Lee, S. T.; Liu, Z. Facile preparation of multifunctional upconversion nanoprobes for multimodal imaging and dual-targeted photothermal therapy. *Angew. Chem Int. Ed.* **2011**, *50*, 7385–7390.

[57] Cheng, L.; Yang, K.; Li, Y.; Zeng, X.; Shao, M.; Lee, S. T.; Liu, Z. Multifunctional nanoparticles for upconversion luminescence/MR multimodal imaging and magnetically targeted photothermal therapy. *Biomaterials*, in press, **2012**,

DOI: 10.1016/j.biomaterials.2011.11.069.

[58] Chertok, B.; David, A. E.; Yang, V. C. Polyethyleneimine-modified iron oxide nanoparticles for brain tumor drug delivery using magnetic targeting and intra-carotid administration. *Biomaterials* **2010**, *31*, 6317–6324.

[59] Huang, X.; Jain, P. K.; El-Sayed, I. H.; El-Sayed, M. A. Plasmonic photothermal therapy (PPTT) using gold nano-particles. *Lasers Med. Sci.* **2008**, *23*, 217–228.

[60] Liu, X.; Tao, H.; Yang, K.; Zhang, S.; Lee, S. T.; Liu, Z. Optimization of surface chemistry on single-walled carbon nanotubes for *in vivo* photothermal ablation of tumors. *Biomaterials* **2011**, *32*, 144–151.

[61] Robinson, J. T.; Welsher, K.; Tabakman, S. M.; Sherlock, S. P.; Wang, H. L.; Luong, R.; Dai, H. J. High performance *in vivo* near-IR (> 1 μm) imaging and photothermal cancer therapy with carbon nanotubes. *Nano Res.* **2010**, *3*, 779–793.